J Solid State Electrochem (2011) 15:2107–2117
DOI 10.1007/s10008-011-1532-3

ORIGINAL PAPER

π-dimerization of pleiadiene radical cations at low temperatures revealed by UV–vis spectroelectrochemistry and quantum theory

Layo van het Goor · Piet Th. van Duijnen · Carola Koper · Leonardus W. Jenneskens · Remco W. A. Havenith · František Hartl

Received: 24 June 2011 / Revised: 21 July 2011 / Accepted: 22 July 2011 / Published online: 6 September 2011

Abstract One-electron oxidation of the non-alternant polycyclic aromatic hydrocarbon pleiadiene and related cyclohepta[*c,d*]pyrene and cyclohepta[*c,d*]fluoranthene in THF produces corresponding radical cations detectable in the temperature range of 293–263 K only on the subsecond time scale of cyclic voltammetry. Although the EPR-active red-coloured pleiadiene radical cation is stable according to the literature in concentrated sulfuric acid, spectroelectrochemical measurements reported in this study provide convincing evidence for its facile conversion into the green-coloured, formally closed shell and, hence, EPR-silent π-bound dimer dication stable in THF at 253 K. The unexpected formation of the thermally unstable dimeric product featuring a characteristic intense low-energy absorption band at 673 nm (1.84 eV; $\log\varepsilon_{max}=4.0$) is substantiated by ab initio calculations on the parent pleiadiene molecule and the PF_6^- salts of the corresponding radical cation and dimer dication. The latter is stabilized with respect to the radical cation by 14.40 kcal mol^{-1} (DFT B3LYP) [37.64 kcal mol^{-1} (CASPT2/DFT B3LYP)]. An excellent match has been obtained between the experimental and TD-DFT-calculated UV–vis spectra of the PF_6^- salt of the pleiadiene dimer dication, considering solvent (THF) effects.

Keywords Pleiadiene · Radical cation · π-Dimerization · Electronic absorption · Quantum chemistry calculations · Polarizable force fields

This article is dedicated to Prof. Fritz Pragst on the occasion of his 70th birthday.

Electronic supplementary material The online version of this article (doi:10.1007/s10008-011-1532-3) contains supplementary material, which is available to authorized users.

L. van het Goor · C. Koper · L. W. Jenneskens (✉)
Organic Chemistry and Catalysis,
Debye Institute for Nanomaterials Science, Utrecht University,
Universiteitsweg 99,
3584 CG Utrecht, The Netherlands
e-mail: l.w.jenneskens@uu.nl

P. T. van Duijnen · R. W. A. Havenith (✉)
Theoretical Chemistry, Zernike Institute for Advanced Materials,
Rijksuniversiteit Groningen,
Nijenborgh 4,
9747 AG Groningen, The Netherlands
e-mail: r.w.a.havenith@rug.nl

F. Hartl (✉)
Department of Chemistry, University of Reading,
Whiteknights,
Reading RG6 6AD, UK
e-mail: f.hartl@reading.ac.uk

Introduction

Although many non-alternant polycyclic aromatic hydrocarbons (PAHs) [1] consisting of an alternant PAH core modified by *peri*-annulation of an unsaturated five-membered ring are known (CP-PAHs, Chart 1: compare **1–3** with **7–9**), [2, 3] the number of available analogues containing a *peri*-annulated unsaturated seven-membered ring instead (CH-PAH, Chart 1: compare **7–9** with **4–6**) is still scarce [4]. This is unfortunate since Michl in 1976 published an imaginative paper [5] providing evidence based on the qualitative PPP theory that the related non-alternant PAHs acenaphthylene (**7**) and pleiadiene (**4**) exhibit a pseudo-alternant relationship. This is due to the existence of approximate mirror–image pairing of the π-MOs and electronic states of **4** and **7**, similar to that found in the case of alternant PAHs [1]. The analysis put forward

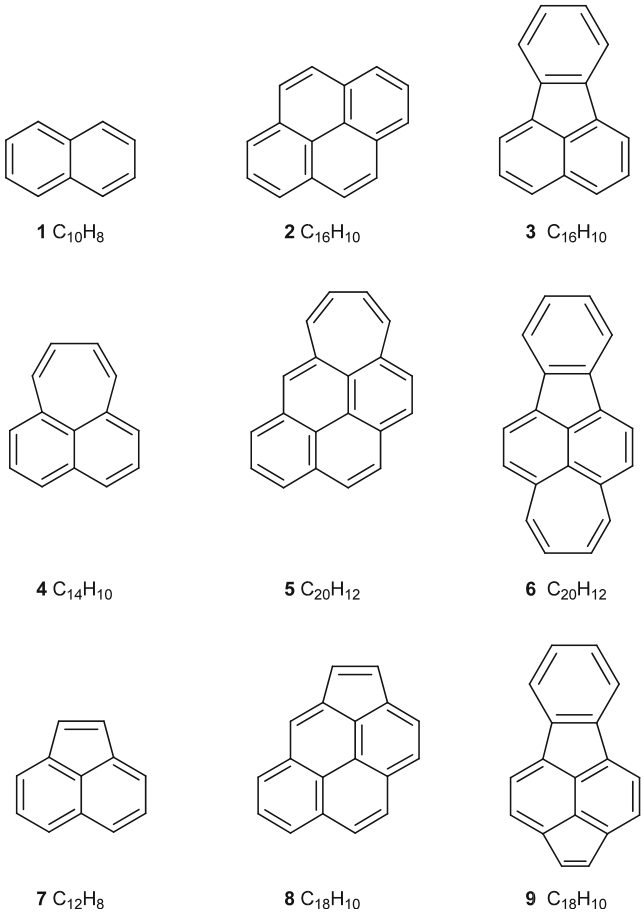

Chart 1 Structures of the alternant PAHs naphthalene (**1**) and pyrene (**2**), the non-alternant PAH fluoranthene (**3**), the non-alternant CH-PAHs pleiadiene (**4**), cyclohepta[*c,d*]pyrene (**5**), and cyclohepta[*c,d*]fluoranthene (**6**), and the non-alternant CP-PAHs acenaphthylene (**7**), cyclopenta[*c,d*]pyrene (**8**), and cyclopenta[*c,d*]fluoranthene (**9**)

by Michl has explained why the UV–vis spectra of **4** and **7** show a striking resemblance (slightly shifted electronic transition energies, intensities, polarizations, and overall band shapes in the 200−900-nm region) [5]. It also accounts for the observation that **7** features a positively shifted (less negative) reduction potential (stabilized LUMO), [6] opposite to **4** with a negatively shifted (less positive) oxidation potential (destabilized HOMO) when compared to the redox potentials of naphthalene (**1**). Concomitant with the occurrence of approximate mirror–image pairing in the case of **4** and **7**, the acenaphthylene radical anion ($\mathbf{7}^{\bullet-}$) and pleiadiene radical cation ($\mathbf{4}^{\bullet+}$) should also possess similar UV–vis spectra as well as similar spin distributions in the naphthalene cores [5] of $\mathbf{4}^{\bullet+}$ and $\mathbf{7}^{\bullet-}$. However, whereas the UV–vis spectrum of $\mathbf{7}^{\bullet-}$ is known [7, 8], that of $\mathbf{4}^{\bullet+}$ has not been reported to date.

Recently, a new synthetic procedure has been developed, providing easier access to pleiadiene (**4**) as well as to the hitherto unknown CH-PAHs cyclohepta[*c,d*]pyrene (**5**) and cyclohepta[*c,d*]fluoranthene (**6**, Chart 1) (van het Goor et al., manuscript in preparation). The so far unpublished study has also briefly dealt with the redox properties of the CH-PAHs and pointed to a limited stability of the corresponding radical cations in acetonitrile (MeCN) at room temperature [4]. Notwithstanding, oxidation of CH-PAHs **4–6** is considerably more facile, i.e. negatively shifted, compared to oxidation of the related (non)-alternant PAH core (Table 1). Indeed, the anodic behaviour of **4–6** shows an approximate mirror–image relationship with the reduction behaviour [4] of the related CP-PAHs **7–9**.

With the general aim to obtain and characterise CH-PAH radical cations $\mathbf{4}^{\bullet+}$–$\mathbf{6}^{\bullet+}$ for the comparative studies with

Table 1 Oxidation potentials and solvent-corrected ionisation potentials[a] of the PAHs **1–3** and the (non-alternant) CH-PAHs **4–6** (see Chart 1)

Compd.	$E_{1/2}(0/+1)$ (V vs. Fc/Fc^+)[b]	ΔE (in V)	$E_{1/2}(0/+1)$ (V vs. Fc/Fc^+)[c]	ΔE (in V)	$IP(0/+1)_{MeCN}$ (eV)	$IP(0/+1)_{THF}$ (eV)
1	1.13				5.87	6.06
2	0.75				5.48	5.65
3	1.04				5.89	6.04
4	0.35	0.10	0.45[e]	0.12	4.93	5.11
5	0.21	0.12	0.34[f]	0.12	4.77	4.95
6	0.44[d]	Irrev.	0.52[g]	0.06	5.04	5.21

Compd. compound, *Irrev.* irreversible

[a] Not corrected for ZPVE (see "Experimental" section)

[b] In MeCN. Converted from the SCE potential scale using $E_{1/2}$ (Fc/Fc^+)=+0.41 V vs. SCE in MeCN. For **1–3**: voltammetry at 293 K on a rotating Pt disc microelectrode [11]. For **4–6**: cyclic voltammetry at 293 K and v=50 mV s^{-1}

[c] In THF. Cyclic voltammetry at v=100 mV s^{-1}

[d] $E_{p,a}$ value

[e] T=293 K

[f] T=273 K; scan rate of 2 V s^{-1}

[g] T=263 K

radical anions of the corresponding CP-PAHs, we wish to present new results of cyclic voltammetric and spectroelectrochemical (UV–vis, EPR) investigations of the parent compounds. This article is focused on the radical cation of pleiadiene ($\mathbf{4}^{\bullet+}$) reported in a preceding EPR spectroscopic study by Murata and co-workers [9]. It is shown that the stability of $\mathbf{4}^{\bullet+}$ is affected by the applied experimental conditions. A compelling evidence based on DFT and TD-DFT calculations is provided for π-dimerization of open shell $\mathbf{4}^{\bullet+}$ into the formally closed-shell $[\mathbf{4}\text{-}\mathbf{4}]^{2+}$ dication.

Results and discussion

Cyclic voltammetry

Oxidation of the CH-PAHs pleiadiene (**4**) and cyclohepta[*c,d*]pyrene (**5**) in MeCN to the corresponding radical cations was shown by Koper to be quasi-reversible at room temperature on the time scale of cyclic voltammetry defined by v= 50 mV s^{-1}, with the peak–current ratio $i_c/i_a<1$ and slightly different shapes of the anodic and cathodic waves of the (0/+1) redox couple [4]. In contrast, oxidation of cyclohepta[*c,d*]fluoranthene (**6**) was completely *irreversible* under these conditions, with the cathodic counter-wave absent on the reverse potential scan. The corresponding anodic potentials are given in Table 1.

The anodic behaviour of the CH-PAHs **4–6** was studied at variable temperature in THF suited also for EPR characterisation of the oxidized products. Table 1 documents that the oxidation potentials are more positive in THF compared to MeCN, in agreement with the calculated higher values of the solvent-corrected adiabatic ionisation potentials of the CH-PAHs in the former less polar solvent (ε_{THF}=7.5 and ε_{MeCN}= 36.6) [10]: $IP(0/+1)_{THF}>IP(0/+1)_{MeCN}$.

The oxidation of pleiadiene (**4**) at ambient temperature is diffusion-controlled and almost chemically reversible ($I_c/I_a\sim$ 1). On the reverse cathodic scan initiated 250 mV beyond the (0/+1) couple of **4** at $E_{1/2}$=0.45 V vs. Fc/Fc^+, two additional peaks are observed at $E_{p,c}$=−0.09 and −0.59 V (Fig. 1a). Their intensities further increased when the potential sweep was held beyond the anodic wave of **4** for 10 s. At T=273 K the radical cation $\mathbf{4}^{\bullet+}$ becomes stable on the subsecond time scale. However, the ΔE_p value is significantly increasing compared to the internal standard, cobaltocene/cobaltocenium, and this trend continues down to 210 K (Fig. 1b–d). The electrochemically quasi-reversible anodic behaviour of **4** may reflect the onset of

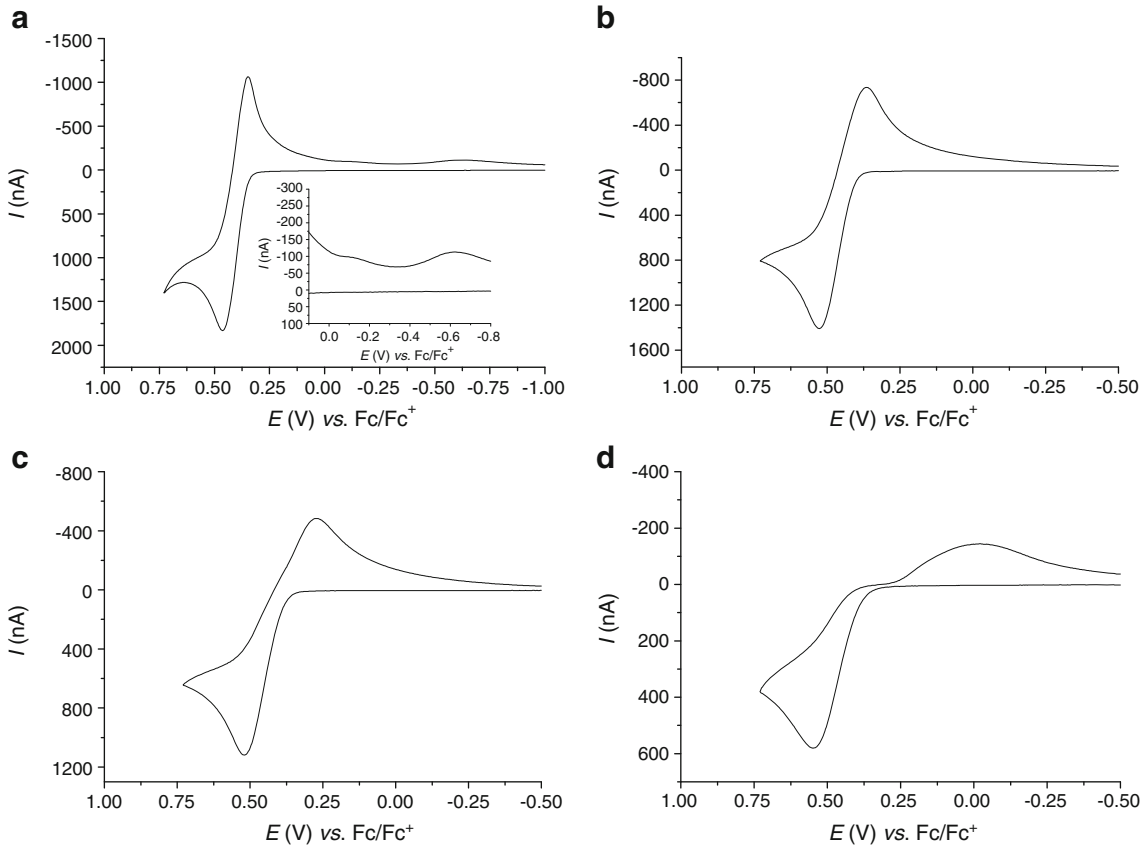

Fig. 1 Cyclic voltammograms of **4** in THF/10^{-1} TBAH at **a** 293 K, **b** 273 K, **c** 243 K, and **d** 210 K. Scan rate v=100 mV s^{-1}, Pt microdisc working electrode

π-dimerization of the radical cations promoted at low temperatures, as revealed by UV–vis spectroelectrochemistry combined with DFT (*vide infra*).

The cyclic voltammetric responses of cyclohepta[*c,d*]pyrene (**5**) and cyclohepta[*c,d*]fluoranthene (**6**) in THF are different in comparison with the oxidation in MeCN (Table 1).

At T=293 K, the oxidation of **5** occurs at $E_{p,a}$=0.41 V vs. Fc/Fc^+ as a totally *irreversible* step (Fig. SI1, see "Supporting Information"). The scan reversal (v=100 mV s^{-1}) beyond the anodic wave was marked by the absence of the cathodic counter peak due to $\mathbf{5}^{\bullet+}$ reduction; instead, it showed reduction of a secondary oxidized product as a broad wave at $E_{p,c}$=−0.04 V vs. Fc/Fc^+, which became more apparent after 10-s electrolysis at 0.6 V. At T=273 K, the cathodic wave at −0.04 V persists in the cyclic voltammogram, but the oxidation of **5** becomes partly chemically *reversible*. Finally, increasing the scan rate to v=2 Vs^{-1} results in the fully *reversible* (0/+1) redox couple of **5** (Table 1; Fig. SI1, see "Supporting Information").

On the contrary, the oxidation of **6** at $E_{1/2}$=0.52 V vs. Fc/Fc^+ is nearly chemically *reversible* already at T=293 K and v=100 mV s^{-1} (Fig. SI2, see "Supporting Information"). On scan reversal, the cathodic response of a secondary oxidized product appears at $E_{p,c}$=−0.46 V, similar to that observed for **4** under these conditions. However, the more positive secondary cathodic wave at ca. −0.05 V, arising at room temperature for oxidized **4** and **5**, was absent in this case. At T=263 K, the oxidation of **6** is fully *reversible* on the subsecond time scale of cyclic voltammetry (Fig. SI2).

UV–Vis spectroelectrochemistry

Figure 2 presents the UV–vis spectra recorded in the course of the spectroelectrochemical oxidation of pleiadiene (**4**) in THF at T=293 and 253 K within an OTTLE cell.

The in situ low-temperature UV–vis spectra show several isobestic points (228, 256, 318, and 380 nm) and a characteristic intense low-energy absorption band of the product at 673 nm (1.84 eV; $\log\varepsilon_{max}$=4.0; Fig. 2b). In agreement with the conventional cyclic voltammograms in Fig. 1c, d, the corresponding thin-layer cyclic voltammogram (TL-CV) showed a fully developed cathodic counter peak on the reverse scan. Upon back reduction, indeed, the spectrum of neutral **4** was fully reproduced.

However, when the oxidation of **4** was conducted at room temperature, the cathodic counter peak in the TL-CV was completely absent. The corresponding UV–vis spectral changes also showed isobestic points (223, 253, 331, and 366 nm), but the low-energy absorption bands in the visible region did not emerge (Fig. 2a). These differences are attributed to the different experimental time scales of the conventional cyclic voltammetry (scan rate of 100 mV s^{-1}) and UV–vis spectroelectrochemistry (scan rate of 2 mV s^{-1}), confirming the reactivity of the green-coloured oxidized species at ambient temperature.

The *reversible* nature of the UV–vis spectral changes and the TL-CV response at 273 K point to generation of stable radical cation $\mathbf{4}^{\bullet+}$. However, the green colour of the product observed at the working electrode, which complies with the visible absorption in Fig. 2a, does not correspond with the literature information according to which the colour of $\mathbf{4}^{\bullet+}$ is deep red when generated in concentrated sulfuric acid [9]. Therefore, we decided to study the green product with EPR spectroscopy (*vide infra*).

In sharp contrast to **4**, oxidations of **5** and **6** both at 253 and 298 K yielded products lacking intense visible absorption above 400 nm in the low-temperature spectra (Figs. SI3 and SI4, see "Supporting Information"). The nature of the UV–vis spectral changes and the absence of cathodic counter peaks along the reverse TL-CV scans clearly indicate that upon oxidation of **5** and **6** on the time

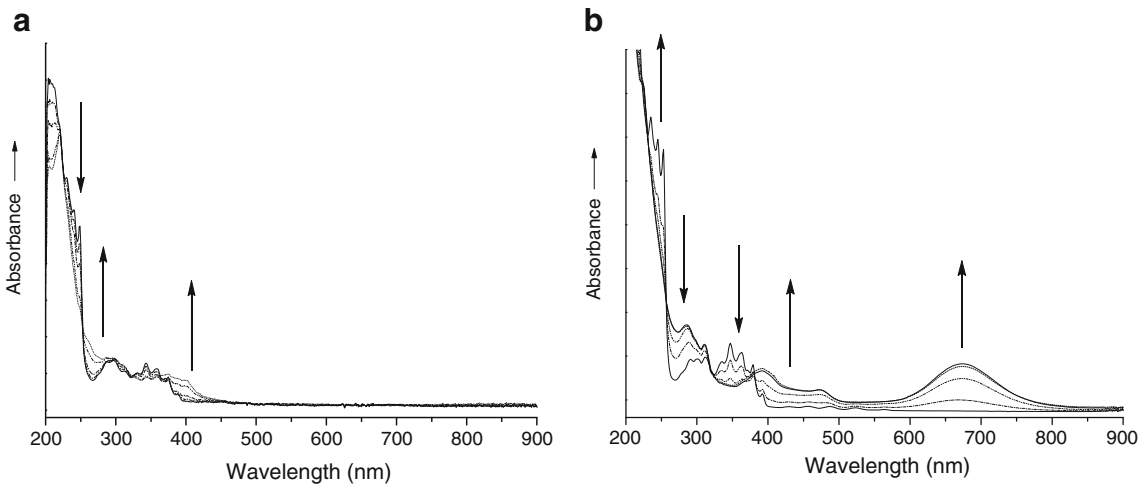

Fig. 2 UV–vis spectra recorded in the course of the in situ oxidation of **4** in THF within an OTTLE cell at T=293 K (**a**) and 253 K (**b**)

scale of minutes other secondary species are formed rather than the desired CH-PAH radical cations. No intense visible absorption band near or above 673 nm is discernible in both cases. Moreover, significant passivation of the working electrode was encountered at low temperatures, presumably due to low solubility of the oxidized products. The spectroelectrochemical study of **5** and **6** was therefore not continued.

EPR spectroscopy

The CV, TL-CV, and UV–vis data have indicated that for most CH-PAHs stable radical cations cannot be obtained in THF at various temperatures, except for pleiadiene (**4**). According to the published results, deep red $\mathbf{4}^{\bullet+}$ was obtained directly after addition of a few drops of H_2SO_4 at room temperature and remained stable for a couple of weeks [9]. The red solution gave a strong EPR signal which could be simulated with five hyperfine splitting constants, in agreement with the symmetric pleiadiene structure (Chart 1).

Nevertheless, attempts to reproduce the experiment of Murata and co-workers [9] were not successful. Addition of a few drops of H_2SO_4 to **4** at room temperature produced the deep red solution of $\mathbf{4}^{\bullet+}$, which, however, turned green within a few seconds. The product was not further analysed. Similarly, when the chemical oxidation of **4** was performed with [$Ce(OTf)_4$] (E_{ox}>0.9 V vs. Fc/Fc^+) [12] in THF at 243 K, a green solution was obtained which did not show any EPR signal. A silent EPR response was also recorded after in situ oxidation of **4** within an EPR spectroelectrochemical cell (see "Experimental") under the same conditions as employed for the low-temperature UV–vis spectroelectrochemistry (Fig. 2a).

From these results it could be deduced that the green solutions did not contain $\mathbf{4}^{\bullet+}$ or any other related paramagnetic species. On the other hand, the quasi-reversible nature of the anodic process, as evidenced by CV and TL-CV at low temperature, excluded any extensive decomposition of the radical cations. An acceptable option has been a conversion of $\mathbf{4}^{\bullet+}$ into more stable π-bound dimer dications, $[\mathbf{4\text{-}4}]^{2+}$, based on analogy with radical cations of tetrathiafulvalene dimerizing at low temperatures [13]. This idea was successfully investigated with quantum chemical methods, including the analysis of the electronic absorption spectrum of the green oxidized species presented in the following section (see Figs. 3b and 5).

Quantum mechanical calculations

Figure 3 shows the experimental UV–vis spectra and the ab initio PCM/B3LYP/TZP vertical excitations of **4** and $\mathbf{4}^{\bullet+}$. Tables 2 and 3 present the PCM/B3LYP/TZP vertical excitations and their assignments, respectively.

The UV–vis spectrum of neutral pleiadiene (**4**) (Fig. 3a) shows a small bathochromic shift of the predicted vertical excitations compared to the experimental absorption maxima. The two absorption bands in the spectrum of pleiadiene (**4**) are mainly characterised by one-electron transitions from the HOMO, e.g., HOMO→LUMO+1. The HOMO→LUMO one-electron transition is predicted at 2.43 eV and is hardly intense, which agrees with the experimental spectrum.

The calculated spectrum for the radical cation $\mathbf{4}^{\bullet+}$ shows little agreement with the experimental spectrum, both in peak positions and intensities (Fig. 3b). Electron excitation from the singly occupied α-HOMO (or SOMO) to the LUMO (Table 3 and Chart SI1, see "Supporting Information") is indeed predicted to occur at a lower energy; however, the calculated oscillator strength is too low. Other weak absorptions involving electron transitions to the SOMO are predicted to occur at low energy. The first intense absorption band is calculated at 2.99 eV, which can be assigned to a mixed α-HOMO→LUMO+1 and β-HOMO-2→SOMO transition (Table 3).

The mismatch between the calculated UV–vis spectrum of $\mathbf{4}^{\bullet+}$ and the experimental spectrum led to a further

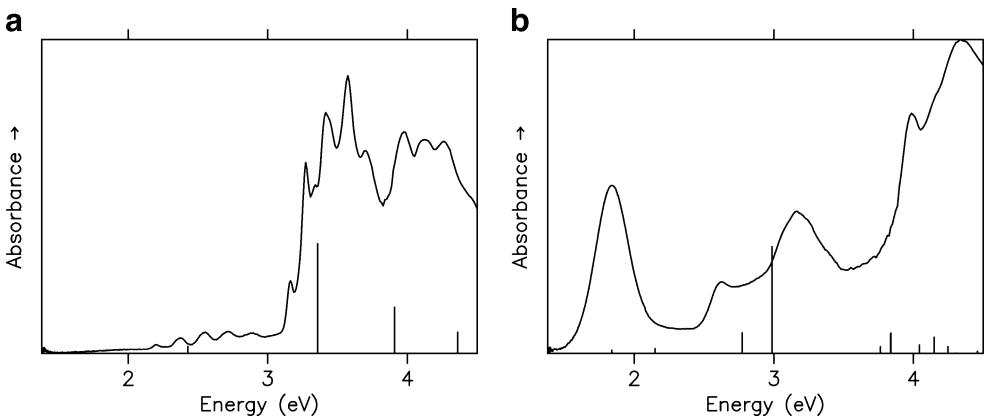

Fig. 3 PCM/B3LYP/TZP vertical excitations of **4** (**a**) and $\mathbf{4}^{\bullet+}$ (**b**) in the range of 1.4–4.5 eV (i.e. 900–275 nm) combined with the corresponding experimental UV–vis spectra (see also Fig. 2)

Table 2 PCM/TD-DFT vertical excitations, excitation energies (λ_{calc}), oscillator strengths (f_{calc}), and the character of the transitions of **4** (C_{2v}) ($|c|>0.45$)

State	λ_{calc} (eV)	Assignment	f_{calc}	λ_{exp} (eV)[a]
1 (B_2)	2.43	HOMO→LUMO	0.014	2.22
2 (A_1)	3.36	HOMO→LUMO+1	0.21	3.20
3 (B_2)	3.91	HOMO→LUMO+2	0.089	3.63
4 (A_1)	4.36	HOMO-1→LUMO	0.057	4.18

λ_{exp} represents experimental absorption maxima

[a] Kolc and Michl [14] (see also Fig. 3a)

exploration of the possibility of the formation of the closed-shell dimer $[\mathbf{4\text{-}4}]^{2+}$. A possible conformation for this dimer dication was found by optimising the geometry of two monomers together with two PF_6^- counterions at the B3LYP/cc-pVDZ level of theory (Fig. 4). A stable conformer was found with a shortest C–C distance of 3.220 Å between the two monomers. At this level of theory, the energy of $[\mathbf{4\text{-}4}](PF_6)_2$ is 14.40 kcal mol^{-1} lower than that of two non-interacting $\mathbf{4}(PF_6)$ molecules (Table 4).

The nature of the dimer dication might suggest that closed-shell DFT is not the appropriate method to treat this system. To probe the validity of the DFT approach, the interaction energy between the two monomers was also calculated using the CASPT2 [16, 17] approach (at the B3LYP optimised geometries). Also, at this level an attractive interaction is found between the two monomers, being even stronger than that evaluated at the B3LYP level (Table 4). Natural orbital occupation numbers of 2.0, 0.0, 1.68, and 0.32 have been found, suggesting that indeed the molecule of $[\mathbf{4\text{-}4}](PF_6)_2$ has some biradical character.

The calculated UV–vis spectrum of the $[\mathbf{4\text{-}4}](PF_6)_2$ (Fig. 5; Table 5) shows a remarkably good match with the experimental data. The intense, broad absorption band at 1.84 eV is correctly predicted. This band is assigned to the HOMO→LUMO transition. The HOMO and LUMO in this case consist of the bonding and antibonding combinations of the singly occupied HOMO of the monomer (Chart SI2, see "Supporting Information"). The less intense absorption bands at 2.62 eV and 3.16 eV can be assigned to the calculated peaks at 2.80 and 3.06/3.37 eV, respectively. The lowest excitation energy has also been evaluated at the CASPT2 level for both $\mathbf{4}(PF_6)$ and $[\mathbf{4\text{-}4}](PF_6)_2$. CASPT2 predicts a low intensity band at 2.05 eV (f_{calc}= 0.005) for $\mathbf{4}(PF_6)$, while for $[\mathbf{4\text{-}4}](PF_6)_2$ a band at 1.94 eV (f_{calc}=0.472) is predicted, which is in line with the TD-DFT data.

Solvent effects on the UV–vis spectrum of $[\mathbf{4\text{-}4}](PF_6)_2$ were further studied at the TD-DFT [18] level using the Discrete Reaction Field (DRF) [19, 20] approach, which takes explicit polarizable solvent molecules into consideration. Figure 6 shows the effect of the solvent as obtained from a single solute/solvent configuration. In the range 1.50–2.75 eV the effect is negligible, but a set of additional excitations is present in THF.

Figure 6b presents 500 ('solvated') QM/MM excitations of 20 randomly chosen solute/solvent configurations from a 20-ps MD production run (red curve in Fig. 6b) as

Table 3 PCM/TD-DFT vertical excitations, excitation energies (λ_{calc}), oscillator strengths (f_{calc}), and the character of the transitions of $\mathbf{4}^{\bullet+}$ (C_{2v}) ($|c|>0.45$)

State	λ_{calc} (eV)	Assignment	f_{calc}	λ_{ref} (eV)[a]
1 (B_2)	1.84	α HOMO→LUMO (0.97)	0.0069	1.79
2 (B_2)	2.15	β HOMO−1→SOMO (0.94)	0.011	2.30
3 (A_1)	2.47	α HOMO→LUMO+1 (0.78) β HOMO−2→SOMO (0.70)	0.0003	
4 (B_2)	2.77	β HOMO−3→SOMO (0.97)	0.045	2.50
5 (A_1)	2.99	α HOMO→LUMO+1 (0.59) β HOMO−2→SOMO (0.68)	0.23	2.91
6 (A_1)	3.58	α HOMO−1→LUMO (0.75) β HOMO−1→LUMO (0.58)	0.0001	3.51
7 (B_2)	3.77	α HOMO−2→LUMO (0.45) α HOMO→LUMO+2 (0.64) β HOMO−2→LUMO (0.61)	0.015	3.59
8 (B_2)	3.83	α HOMO−2→LUMO (0.47) α HOMO→LUMO+2 (0.67)	0.044	–
9 (A_1)	4.04	α HOMO−3→LUMO (0.67) β HOMO−3→LUMO (0.62)	0.019	
10 (A_1)	4.15	α HOMO−1→LUMO (0.62) β HOMO−2→LUMO (0.71)	0.035	

λ_{ref} represents other ab initio vertical excitations from the literature

[a] For recent BLYP/6-31 G** data [15]

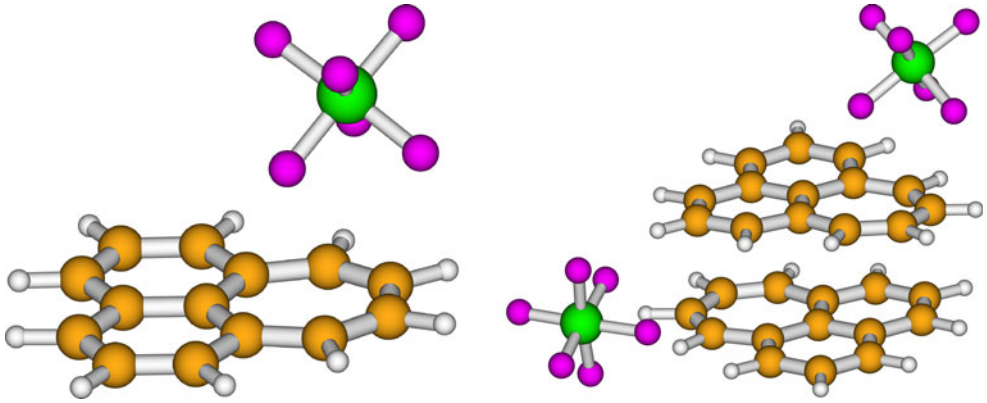

Fig. 4 The B3LYP/cc-pVDZ optimised geometry of **4**(PF_6) and [**4-4**](PF_6)$_2$

generated by applying the DRF90 suite [21]. It shows the naturally growing bands due to the different geometries of the various solute/solvent configurations. The black curve in Fig. 6b is the result of applying a 'virtual spectrometer', i.e. collecting the excitations in 200 boxes having a width of ca. 0.016 eV, and adding up the collected oscillator strengths in each box (the number of boxes and the difference between the largest and smallest excitations defining the resolution). Finally, the blue curve in Fig. 6b is the result of convoluting the 200 peaks of the boxes by Gaussians of ca. 0.1-eV width, simulating the effect of vibrations in the solute molecule. (Convoluting first the 'raw levels' (red curve in Fig. 6b) and then applying the virtual spectrometer give the same result.)

Figure 6c contains a comparison of the result of the preceding panel and the experimental spectrum. First we note that the excitations agree fairly: differences of ca. 0.1 eV in the low-energy regime, and of ca. 0.5 eV in the high-energy range are supposed to be 'normal' for TD-DFT applications [22]. As with the intensities, the differences may be due to the relatively small number of solute/solvent configurations accounted for. Nonetheless, the pattern definitely shows that the experimental spectrum can be attributed to [**4-4**](PF_6)$_2$.

Conclusions

Cyclic voltammetry and, in particular, UV–vis spectroelectrochemistry, have revealed thermal instability of radical cations formed by one-electron oxidation of cyclohepta[*c,d*]pyrene (**5**) and cyclohepta[*c,d*]fluoranthene (**6**) at moderate temperatures, both in THF and MeCN [4]. On the other hand, the radical cation of pleiadiene (**4**) has been characterised by EPR spectroscopy; although the literature preparative method (dissolving crystals of **4** in concentrated sulfuric acid) [9] differs strongly from experimental conditions in this work, viz. electrolysis in organic solvents, the red colour of $\mathbf{4}^{\bullet+}$ is not in contrast with the TD-DFT calculations predicting, after a λ_{calc}-to-λ_{exp} correction of 0.25 eV to the HOMO→LUMO transition energy in Table 3 taken from Table 5, a visible absorption around 550 nm. Cyclic voltammetry points to stability of $\mathbf{4}^{\bullet+}$ in THF/Bu_4NPF_6 at low temperatures below 273 K. However, the analysis of experimental UV–vis spectroelectrochemical data in conjunction with DFT and TD-DFT calculations has provided a compelling evidence for π-dimerization of $\mathbf{4}^{\bullet+}$ at low temperatures and formation of EPR-silent green dimer [**4-4**](PF_6)$_2$. The formally closed-shell dimer dication is strongly stabilized with respect to monomer **4**(PF_6) by 14.40 or even 37.64 kcal mol^{-1} based on DFT B3LYP and CASPT2/DFT B3LYP calculations, respectively. The electronic absorption spectrum of [**4-4**](PF_6)$_2$ has been perfectly

Table 4 Energies (Hartree) of the monomer **4**(PF_6) and dimer [**4-4**](PF_6)$_2$ and the interaction energy ΔE_{int} (kcal mol^{-1}) evaluated at DFT B3LYP/cc-pVDZ and CASPT2 levels of theory

Method	**4**(PF_6)	[**4-4**](PF_6)$_2$	ΔE_{int}
B3LYP	−1480.031671	−2960.086288	−14.40
CASPT2	−1476.565890	−2953.191770	−37.64

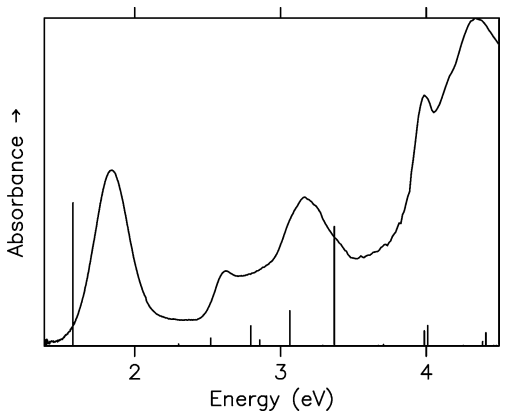

Fig. 5 The PCM/TD-DFT spectrum of [**4-4**](PF_6)$_2$ together with the experimental UV–vis spectrum (see also Fig. 3b)

Table 5 PCM/TD-DFT vertical excitations, excitation energies (λ_{calc}), oscillator strengths (f_{calc}), and the character of the transitions of the π-dimer $[\mathbf{4\text{-}4}]^{2+}$ (C_1) ($|c|>0.45$)

State	λ_{calc} (eV)	Assignment[a]	f_{calc}	λ_{exp} (eV)[b]
1	1.58	HOMO→LUMO	0.293	1.84
2	2.30	HOMO−1→LUMO	0.004	
3	2.35	HOMO→LUMO+1	0.000	
4	2.52	HOMO→LUMO+2	0.016	
5	2.80	HOMO-2→LUMO	0.041	2.62
6	2.86	HOMO−3→LUMO (0.77) HOMO−4→LUMO (0.47)	0.012	
7	3.06	HOMO−4→LUMO (0.81) HOMO−3→LUMO (0.50)	0.072	3.16
8	3.29	HOMO→LUMO+4	0.001	
9	3.37	HOMO→LUMO+3	0.245	

λ_{exp} represents experimental absorption maxima

[a]The MOs involved in the optical transitions 1–9 are depicted in Chart SI2 (see "Supporting Information")

[b]See Figs. 5 and 6

matched by the PCM/TD-DFT-calculated vertical excitations, considering solvent/solute interactions. The green colour of $[\mathbf{4\text{-}4}](PF_6)_2$ arises from the characteristic intense HOMO→LUMO absorption at 673 nm (1.84 eV), which is red-shifted with respect to the visible absorption of $\mathbf{4}^{\bullet+}$. It is noteworthy that a similar behaviour has been reported for the π-dimer of tetrathiafulvalene radical cations [13], forming below 265 K. The results of the present study bring a new view on the anodic behaviour of non-alternant polycyclic hydrocarbons.

Experimental

Syntheses

The CH-PAHs were synthesized following the procedures reported by Koper [4]. Full synthetic details will be reported elsewhere [van het Goor et al., manuscript in preparation].

Caution: (non)-alternant PAHs are potential genotoxic compounds and should be handled with care [23, 24].

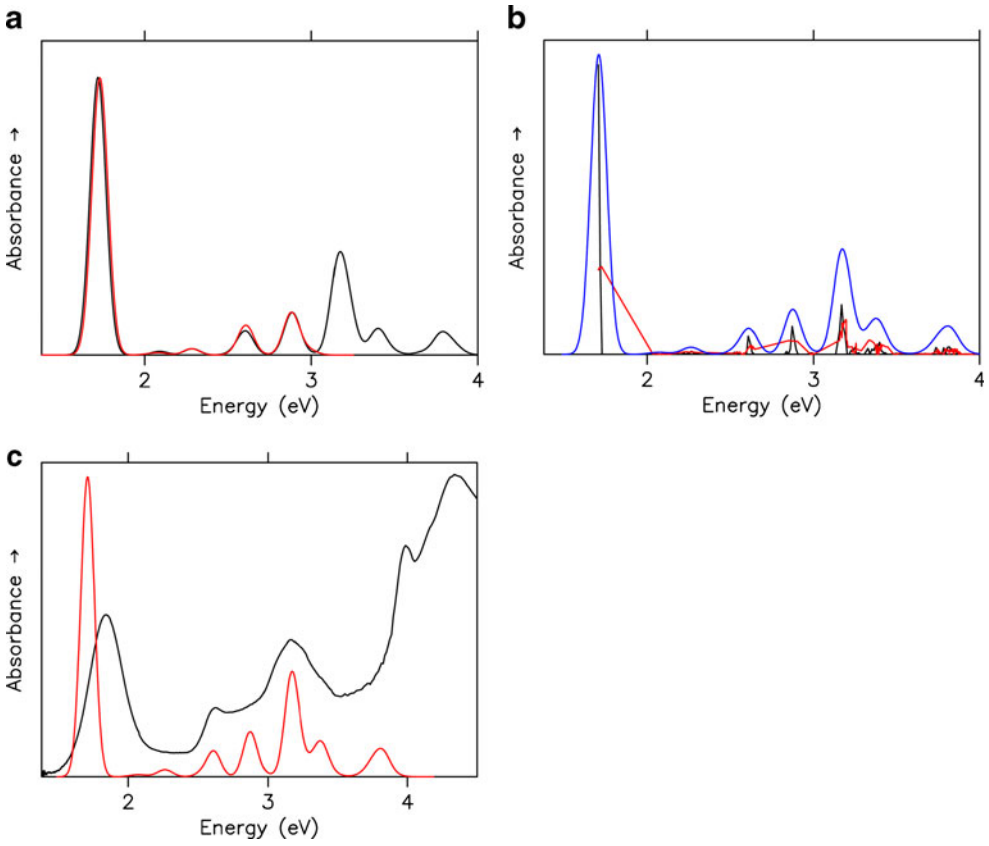

Fig. 6 Solvent effects on the UV–vis spectrum of $[\mathbf{4\text{-}4}](PF_6)_2$. **a** Calculated spectrum of the dimer dication in vacuum (*red*) and in a single solute/solvent configuration (*black*) in 300 THF molecules. **b** Red spectrum: all 500 excitations; black spectrum: 200 excitations collected in boxes 0.016 eV wide; blue spectrum: each of the 200 boxes convoluted with Gaussians. **c** Comparison of the calculated spectrum (*red*) with the experimental spectrum (*black*)

Analytical methods

Electrolytes were purchased from Aldrich and purified according to standard procedures prior to use. Solvents were dried and purified using standard procedures. Commercially available reagents were used without further purification.

Cyclic voltammetry

Conventional cyclic voltammetry (CV) was performed in a Faraday cage, using an air-tight single-compartment three-electrode cell containing a carefully polished Pt microdisc (0.14 mm^2), Pt coil, and Ag coil working, counter, and pseudo-reference electrodes, respectively. The working electrode potential was controlled with an EG&G PAR 283 potentiostat. All electrochemical samples were approximately 10^{-3} M in the studied analyte and 10^{-1} M in the supporting electrolyte (Bu_4NPF_6; dried at 80 °C under vacuum overnight) dissolved in dry THF (distilled from Na wire prior to use). Cobaltocenium hexafluorophosphate was used as an internal reference [12]: $E_{1/2}$=−1.33 V vs. Fc/Fc^+.

UV–Vis spectroelectrochemistry

UV–vis spectroelectrochemical experiments at T=253 K were performed with a cryostatted optically transparent thin-layer electrochemical (OTTLE) cell (0.2-mm optical path length) equipped with CaF_2 windows, a Pt minigrid working electrode (32 wires per centimeter), and Pt auxiliary minigrid electrodes [25, 26]. All electrochemical samples were approximately 10^{-3} M in the studied analyte and 10^{-1} M in the supporting electrolyte (Bu_4NPF_6). The spectroelectrochemical analyses were performed under a nitrogen atmosphere in THF freshly distilled from Na wire. The working electrode potential of the spectroelectrochemical cell was controlled with a PA4 potentiostat (EKOM, Polná, Czech Republic). In situ UV–vis spectra were recorded on a Perkin Elmer Lambda 900 spectrophotometer.

All UV–vis spectroelectrochemical experiments at room temperature were performed with an optically transparent thin-layer electrochemical (OTTLE) [27] cell (0.2-mm optical path length, CaF_2 windows) equipped with Au minigrid working, Pt minigrid auxiliary, and Ag wire pseudo-reference electrodes. The controlled-potential electrolyses were carried out with a PA4 potentiostat (EKOM, Polná, Czech Republic). The potential scan rate was typically 2 mV s^{-1}. All electrochemical samples in dry THF were approximately 10^{-3} M in the studied analyte and contained 10^{-1} M Bu_4NPF_6. The in situ UV–vis spectra were recorded on a Hewlett-Packard 8453 diode-array spectrophotometer.

EPR spectroscopy

Pleiadiene was oxidized in THF under an atmosphere of dry nitrogen within a tubular air-tight electrochemical EPR cell containing outer Au helix working electrode, inner Pt helix counter electrode, and a single-point Ag wire pseudo-reference electrode [28]. The working electrode potential was controlled with a PA4 potentiostat (EKOM, Polná, Czech Republic). The sample was approximately 10^{-4} M in **4** and 10^{-3} M in Bu_4NPF_6.

X-band EPR spectroscopic measurements were carried out with a Varian E104A Century Series EPR spectrometer at 230–250 K. The magnetic field was calibrated against 1,1-diphenyl-2-picrylhydrazyl (g=2.0037, H=3386 G).

Computational methods

Geometry optimisation of the neutral CH-PAHs was performed at the DFT B3LYP [29, 30] level of theory employing the TZP basis set (Todorov et al., manuscript in preparation) using GAMESS-UK [31]. For the open-shell radical cation systems Gaussian03 was utilised [32]. The TZP basis set is based on Dunning's non-augmented TZ basis set [33] modified with p-polarisation functions for the hydrogen atoms (α_p=0.75) and d-polarisation functions for the carbon atoms (α_d=0.60). Solvent-corrected vertical excitations were calculated from the (U)B3LYP/TZP optimised geometries in single-point PCM [34] calculations [32] in Gaussian03.

Hessian calculations showed that the optimised gas phase geometries are proper minima and that no symmetry breaking occurs upon removal of electrons. Furthermore, the structural changes upon oxidation to the radical cations are small. As expected, only a strong antibonding character along the ethene-like bond is observed as a result of lengthening of the olefinic carbon–carbon bond. Optimised geometries and (solvent-corrected) total energies are electronically available.

Solvent-corrected adiabatic ionisation potentials (IP(0/+1), in electronvolt) were computed as energy differences (ΔE_{tot}) between the total energies of the radical cations and the corresponding neutral species in their respective (DFT) PCM/(U)BLYP/TZP optimised geometries (ΔE method; Eq. 1) without ZPVE corrections. Tetrahydrofuran (THF, ε=7.5) [10] and acetonitrile (MeCN, ε=36.6) [10] were used as solvents.

$$\mathrm{IP}(0/+1) = (E_{\mathrm{tot}})_{\text{radical cation}} - (E_{\mathrm{tot}})_{\text{neutral}} = (\Delta E_{\mathrm{tot}})_{\text{radical cation}-\text{neutral}} \quad (1)$$

Solvent-corrected vertical excitations were calculated from the PCM [35, 36]/(U)B3LYP/TZP (Todorov et al., manuscript in preparation) [29, 30], optimised geometries using Gaussian03 with THF as solvent [32].

The geometries of the dimer formed of two radical cations of pleiadiene, [**4-4**]$(PF_6)_2$ and the monomer **4**(PF_6),

were optimised at the B3LYP/cc-pVDZ [33] level of theory, using GAMESS-UK [31]. TD-DFT calculations including solvent effects (PCM, solvent THF) were performed with GAMESS-US [35–37] using the B3LYP functional and the TZP basis set for C and H, and the DZP basis set of Dunning [38, 39] for P and F. CASPT2 [16, 17] calculations were also performed on the B3LYP/cc-pVDZ [33] optimised geometries with MOLCAS 7 using the cc-pVDZ basis set [40]. For the π-dimer, the CASSCF space consisted of 14 electrons in 14 π-like orbitals; for the monomer, the CASSCF space consisted of 7 electrons in 7 π-like orbitals. State-averaged CASSCF calculations over ten and five roots for the dimer and monomer, respectively, were performed.

To assess the effect of the solvent, ADF [18]/TD-DFT with a DZP basis of Slater orbitals was applied. A vacuum calculation gave a point charge representation of the charge distribution preserving up to the quadrupole moment [41]. The charges were used as inputs for Molecular Dynamics (MD) simulations, using the DRF90 suite [42]. The latter is based on a fully polarizable force field, which allows mixed quantum-classical (QM/MM) calculations with the same force field parameters [19, 20]. The polarizabilities were taken as the defaults [42] in DRF90.

The simulation was done at 298 K controlled by a Nosé-Hoover thermostat [43], with a time step of 1 fs in an NTV ensemble of the pleiadiene dimer dication immersed in 300 THF molecules (all molecules treated as rigid). After equilibration, 25 randomly chosen solute/solvent configurations from a 20-ps production run were taken to perform QM/MM (ADF–TD-DFT–DRF) calculations on the 20 lowest allowed excitations. This number of solute/solvent configurations is probably sufficient for our present purposes [44].

Acknowledgements R.W.A.H. acknowledges Prof. Dr. R. Broer (University of Groningen, The Netherlands) for fruitful discussions and the Netherlands Organisation for Scientific Research (NWO) for financial support (the ECHO-grant 700.57.027). Mr. C. Mahabiersing (University of Amsterdam, The Netherlands) is thanked for his assistance with the spectroelectrochemical experiments.

References

1. Streitwieser A (1961) Molecular orbital theory for organic chemists. Wiley, New York
2. Jenneskens LW, Sarobe M, Zwikker JW (1996) Pure Appl Chem 96:291–300
3. Scott LT (1996) Pure Appl Chem 96:291–300
4. Koper C PhD (2003) Non-alternant polycyclic aromatic hydrocarbons versus closed carbon surfaces. Thesis, Utrecht University, Utrecht
5. Michl J (1976) J Am Chem Soc 98:4546–4549
6. Koper C, Sarobe M, Jenneskens LW (2004) Phys Chem Chem Phys 6:319–327
7. Zahradník R, Rejholec P, Hobza P, Čársky P, Hafner K (1972) Coll Czech Chem Commun 37:1983–1989
8. Shida T, Iwate S (1973) J Am Chem Soc 95:3473–3483
9. Ikegami Y, Iwaizumi M, Murata I (1974) Chem Lett 1141–1144
10. Lide DR (1994) CRC handbook of chemistry and physics, 75th edn. CRC, Boca Raton
11. Pysh ES, Yang NC (1963) J Am Chem Soc 85:2124–2130
12. Conelly NG, Geiger WE (1996) Chem Rev 96:877–910
13. Khodorkovsky V, Shapiro L, Krief P, Shames A, Mabon G, Gorgues A, Giffard M (2001) Chem Commun 2736–2737
14. Kolc J, Michl J (1976) J Am Chem Soc 98:4540–4545
15. Hirata S, Head-Gordon M, Szczepanski J, Vala M (2003) J Phys Chem A 107:4940–4951
16. Andersson K, Malmqvist P-Å, Roos BOJ (1992) Chem Phys 96:1218
17. Andersson K, Malmqvist P-Å, Roos BO, Sadlej AJ, Wolinski K (1990) J Phys Chem 94:5483–5488
18. SCM (2006) Amsterdam density functional theory, 1st edn. URL http://www.scm.com: Amsterdam
19. de Vries AH, van Duijnen PTh, Juffer AH, Rullmann JAC, Dijkman JP, Merenga H, Thole BT (1995) J Comput Chem 16:37–55
20. van Duijnen PTh, Swart M, Jensen L (2008) The discrete reaction field approach for calculating solvent effects. In: Canuto S (ed) Solvation effects on molecules and biomolecules: computational methods and applications, vol. 6. Springer, Berlin, p 39
21. Swart M, van Duijnen PTh (2006) Mol Simul 32:471–484
22. van Gisbergen SJA, Snijders JG, Baerends EJ (1999) Comp Phys Commun 118:119–138
23. Otero-Lobato M-J, Jenneskens LW, Seinen W (2004) Mut Res 559:105–119
24. Otero-Lobato M-J, Kaats-Richter VEM, Koper C, Vlietstra EJ, Havenith RWA, Jenneskens LW, Seinen W (2005) Mut Res 582:115–132
25. Mahabiersing T, Luyten H, Nieuwendam RC, Hartl F (2003) Collect Czech Chem Commun 68:1687–1709
26. Hartl F, Luyten H, Nieuwenhuis HA, Schoemaker GC (1994) Appl Spectroscopy 48:1522–1528
27. Krejčík M, Daněk M, Hartl F (1991) J Electroanal Chem Interfacial Electrochem 317:179–187
28. Hartl F, Groenestein RP, Mahabiersing T (2001) Collect Czech Chem Commun 66:52–66
29. Becke AD (1994) J Chem Phys 98:5648–5652
30. Lee C, Yang W, Parr RG (1988) Phys Rev B 37:785–789
31. Guest MF, Bush IJ, van Dam HJJ, Sherwood P, Thomas JMH, van Lenthe JH, Havenith RWA, Kendrick J (2005) Mol Phys 103:719–747
32. Frisch MJ, Trucks GW, Schlegel HB, Scuseria GE, Robb MA, Cheeseman JR, Montgomery JJA, Vreven T, Kudin KN, Burant JC, Millam JM, Iyengar SS, Tomasi J, Barone V, Mennucci B, Cossi M, Scalmani G, Rega N, Petersson GA, Nakatsuji H, Hada M, Ehara M, Toyota K, Fukuda R, Hasegawa J, Ishida M, Nakajima T, Honda Y, Kitao O, Nakai H, Klene M, Li X, Knox JE, Hratchian HP, Cross JB, Bakken V, Adamo C, Jaramillo J, Gomperts R, Stratmann RE, Yazyev O, Austin AJ, Cammi R, Pomelli C, Ochterski JW, Ayala PY, Morokuma K, Voth GA, Salvador P, Dannenberg JJ, Zakrzewski VG, Dapprich S, Daniels AD, Strain MC, Farkas O, Malick DK, Rabuck AD, Raghavachari K, Foresman JB, Ortiz JV, Cui Q, Baboul AG, Clifford S, Cioslowski J, Stefanov BB, Liu G, Liashenko A, Piskorz P, Komaromi I, Martin RL, Fox DJ, Keith T, Al-Laham MA, Peng CY, Nanayakkara A, Challacombe M, Gill PMW, Johnson B, Chen W, Wong MW, Gonzalez C, Pople JA (2004) Gaussian 03, revision D.01. Gaussian, Pittsburg
33. Dunning TH (1971) J Chem Phys 33:716–723
34. Tomasi J, Mennucci B, Cammi R (2005) Chem Rev 105:2999–3094
35. Schmidt MW, Baldridge KK, Boatz JA, Elbert ST, Gordon MS, Jensen JJ, Koseki S, Matsunaga N, Nguyen KA, Su S, Windus

TL, Dupuis M, Montgomery JA (1993) J Comput Chem 14:1347–1363
36. Gordon MS, Schmidt MW (2005) In: Dykstra CE, Frenking G, Kim KS, Scuseria GE (eds) Theory and applications of computational chemistry, the first forty years. Elsevier, Amsterdam, pp 1167–1189
37. Tawada Y, Tsuneda T, Yanagisawa S, Yanai Y, Hirao K (2004) J Chem Phys 120:8425–8433
38. Dunning TH, Hay PJ (1977) In: Methods of electronic structure theory, vol. 2. Schaefer III HF (ed) Plenum
39. Magnusson E, Schaefer HF III (1985) J Chem Phys 83:5721–5726
40. Aquilante F, De Vico L, Ferré N, Ghigo G, Malmqvist P-Å, Neogrády P, Bondo PT, Pitoňák M, Reiher M, Roos BO, Serrano-Andrés L, Urban M, Veryazov V, Lindh R (2010) J Comput Chem 31:224–247
41. Swart M, van Duijnen PTh, Snijders JG (2001) J Comp Chem 22:79–88
42. Swart M, van Duijnen PTh (2006) Mol Simul 32:471–484
43. Toxvaerd T (1972) Mol Phys 72:159–168
44. Coutinho K, Oliveira MJD, Canuto S (1998) Int J Quantum Chem 66:249–253